Supporting Information for

Magic Angle Spinning NMR Reveals Sequence-Dependent Structural Plasticity, Dynamics, and the Spacer Peptide 1 Conformation in HIV-1 Capsid Protein Assemblies

Yun Han[1,2#], Guangjin Hou[1,2#], Christopher L. Suiter[1,2], Jinwoo Ahn[1,3], In-Ja L. Byeon[1,3], Andrew S. Lipton[4], Sarah Burton[4], Ivan Hung[5], Peter L. Gor'kov[5], Zhehong Gan[5], William Brey[5], David Rice[6], Angela M. Gronenborn[1,3], and Tatyana Polenova[1,2]*

[1]*Department of Chemistry and Biochemistry, University of Delaware, Newark, DE 19716, United States;*
[2]*Pittsburgh Center for HIV Protein Interactions, University of Pittsburgh School of Medicine, Pittsburgh, PA 15261, United States;*
[3]*Department of Structural Biology, University of Pittsburgh School of Medicine, 3501 Fifth Ave., Pittsburgh, PA 15261, United States;*
[4]*Environmental Molecular Sciences Laboratory, Pacific Northwest National Laboratory, Richland, WA, 99352, United States;*
[5]*Nuclear Magnetic Resonance Program, National High Magnetic Field Laboratory, Tallahassee, FL, 32310, United States;*
[6]*Agilent Technologies, Inc., 5301 Stevens Creek Boulevard, Santa Clara, CA 95051; United States.*
[#]*These authors contributed equally to this work*

E-mail: tpolenov@udel.edu

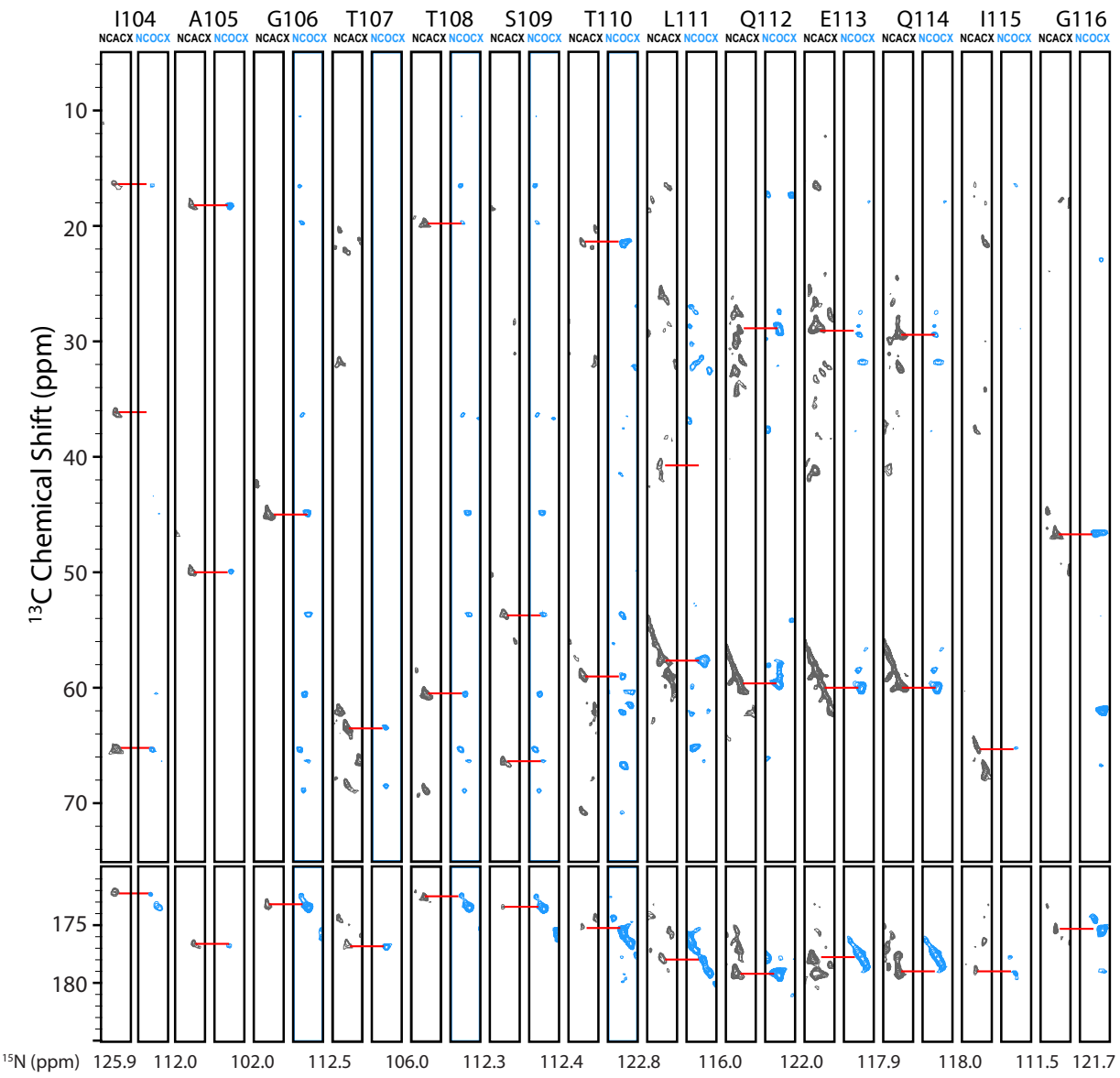

Figure S1. Backbone walk for the R100-G116 stretch of residues of tubular assemblies of U-^{13}C,^{15}N HIV-1 CA WT (HXB2 strain) generated from the 3D NCACX and NCOCX spectra acquired at 21.1 T and 4 °C. The acquisition parameters are given in the Supporting Information.

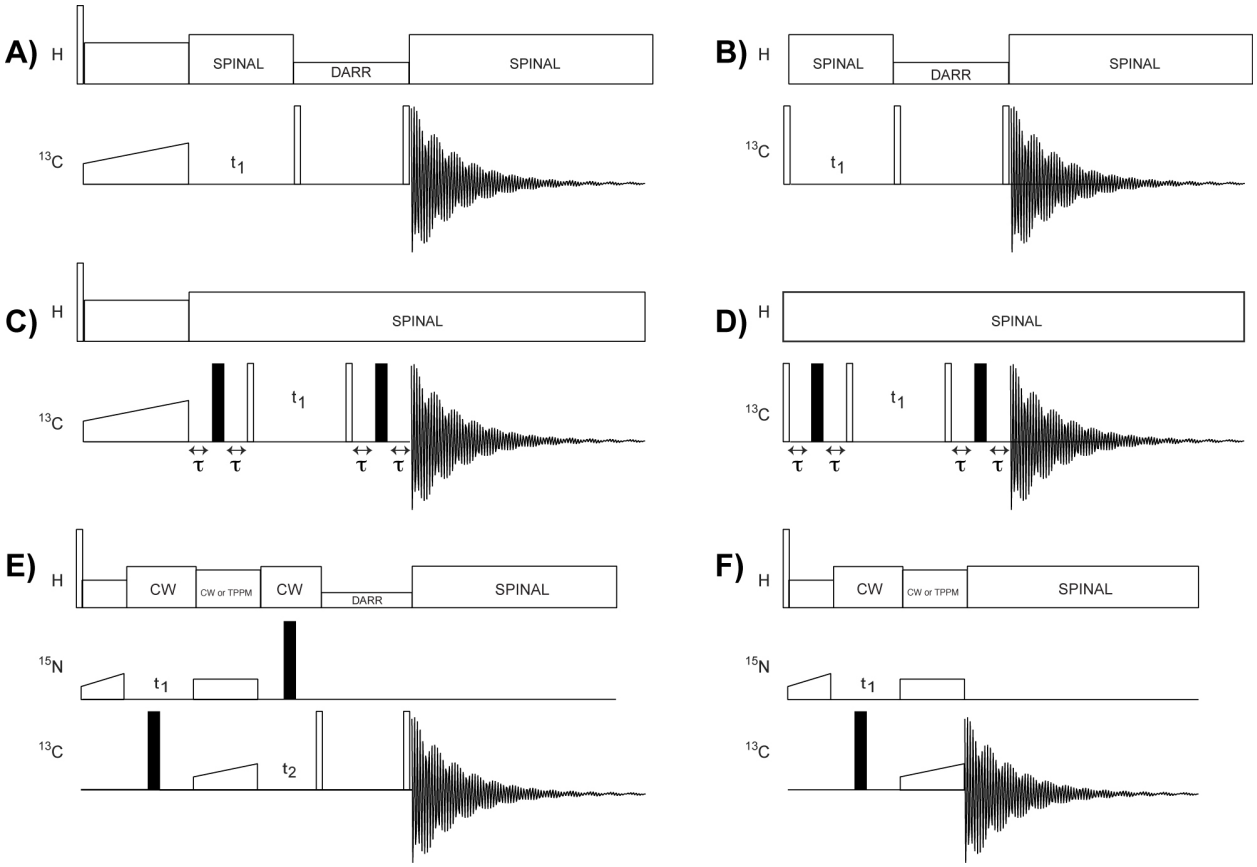

Figure S2. Diagrams of pulse sequences used in this work: A) CP-DARR; B) direct-DARR; C) CP-INADEQUATE; D) direct-INADEQUATE; E) NCACX/NCOCX; and F) NCA.

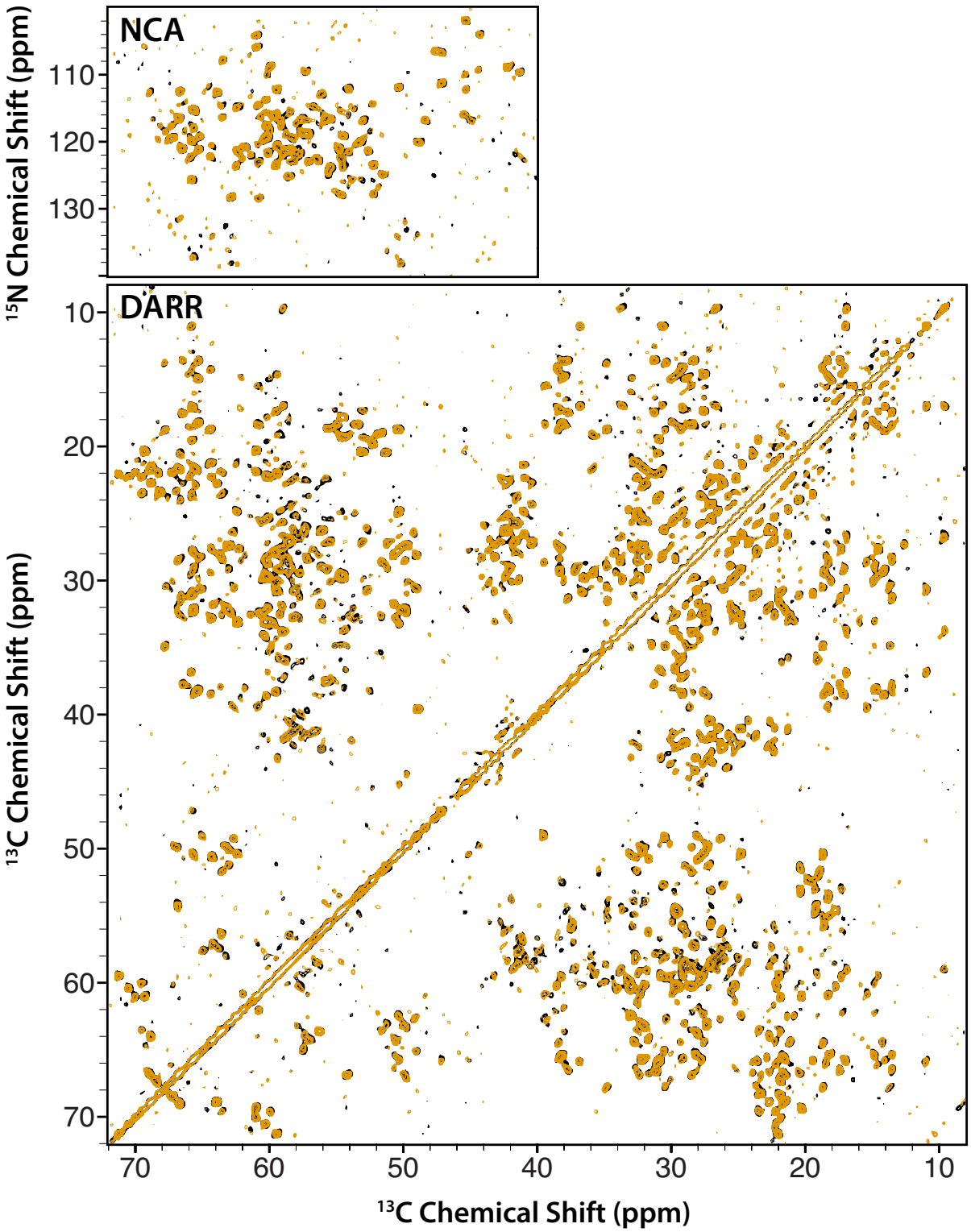

Figure S3. The superposition of the NCA (top) and aliphatic region of CP-DARR (bottom) spectra of tubular assemblies acquired at 19.9 T and 4 °C. CA NL4-3 A92E is in orange and CA-SP1 NL4-3 A92E is in black. The DARR mixing time was 50 ms. The acquisition parameters for the spectra of U-^{13}C,^{15}N HIV-1 CA-SP1 tubular assemblies are given in Table S1.

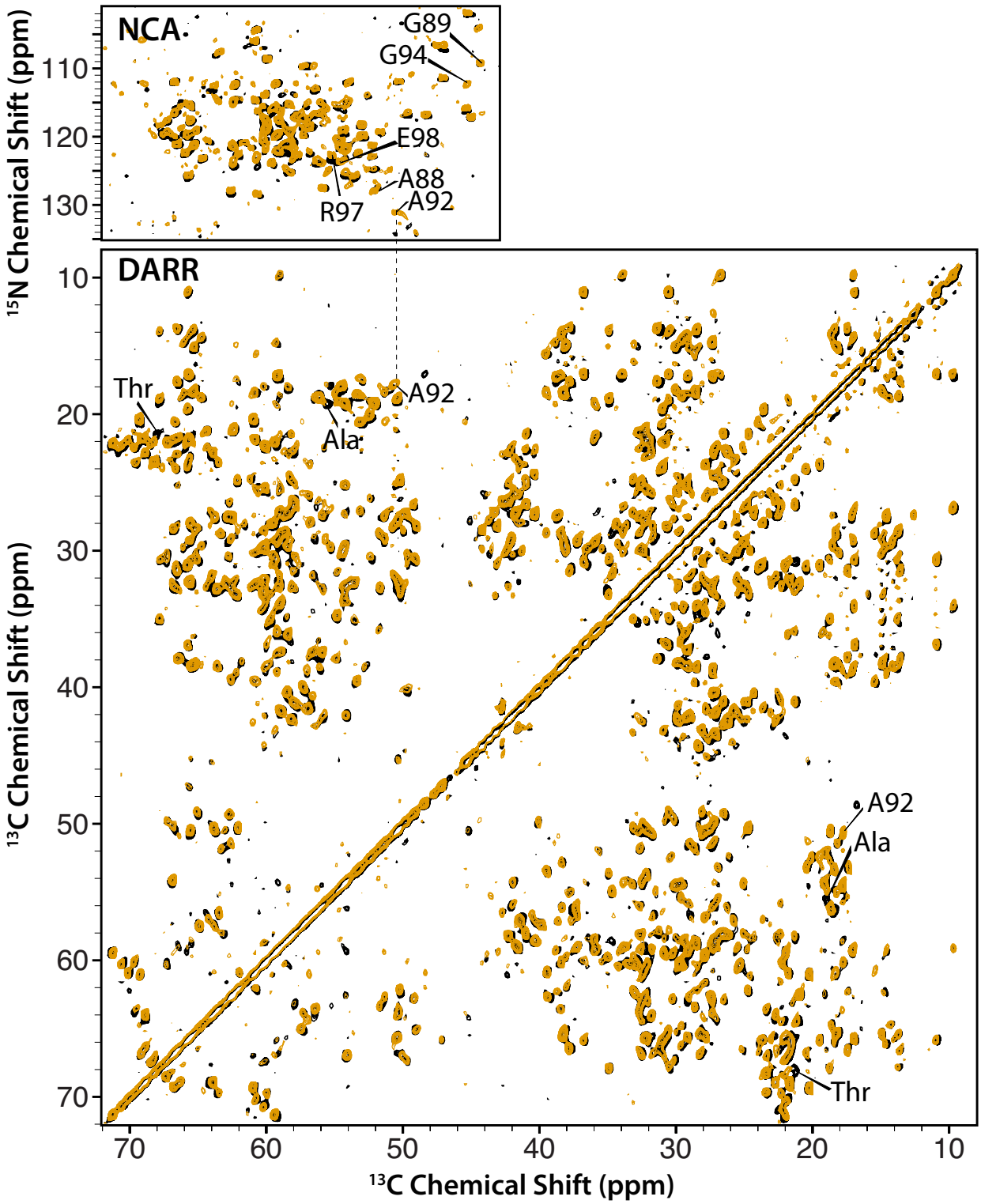

Figure S4. The superposition comparison of the NCA (top) aliphatic region of CP-DARR (bottom) spectra acquired at 21.1 T and 4 °C. CA HXB2 is in orange and CA-SP1 HXB2 is in black. The DARR mixing time was 50ms. The acquisition parameters for the spectra of U-^{13}C,^{15}N HIV-1 CA-SP1 tubular assemblies are given in Table S1.

Table S1. Acquisition and processing parameters for the solid-state NMR experiments in tubular assemblies of CA and CA-SP1.

Experiment	Acquisition			Processing		
	ω3	ω2	ω1	ω3	ω2	ω1
19.9 T						
U-^{13}C,^{15}N-CA, NL4-3 A92E variant						
CP-DARR (τ_{mix}=50 ms)		1024 complex; SW = 64 kHz, 128 scans	512 real, SW = 45 kHz		30-degree sinebell; Lorentzian-to-Gaussian transformation	forward linear prediction of 512 points; 30-degree sinebell; Lorentzian-to-Gaussian transformation
direct-DARR(τ_{mix}=50 ms)		1024 complex; SW =64 kHz, 192 scans	400 real, SW = 45 kHz		30-degree sinebell; Lorentzian-to-Gaussian transformation	forward linear prediction of 512 points; 30-degree sinebell; Lorentzian-to-Gaussian transformation
NCACX		1024 complex; SW =85.2 kHz, 2896 scans	64 complex; (States) SW=6.5 kHz		30-degree sinebell; Lorentzian-to-Gaussian transformation	forward linear prediction of 64 points; 30-degree sinebell; Lorentzian-to-Gaussian transformation
NCA		1024 complex; SW =85.2 kHz, 320 scans	44 complex; (TPPI) SW=6.5 kHz		30-degree sinebell; Lorentzian-to-Gaussian transformation	forward linear prediction of 128 points; 30-degree sinebell; Lorentzian-to-Gaussian transformation
NCOCX		1024 complex; SW =64 kHz, 1360 scans	40 complex; (TPPI) SW=5 kHz		30-degree sinebell; Lorentzian-to-Gaussian transformation	forward linear prediction of 128 points; 30-degree sinebell; Lorentzian-to-Gaussian transformation
CP-INADEQUATE		1024 complex; SW =64 kHz, 416 scans	400 real; (TPPI) SW=81 kHz		60-degree sinebell; Lorentzian-to-Gaussian transformation	forward linear prediction of 1024 points; 60-degree sinebell; Lorentzian-to-Gaussian transformation
INADEQUATE		1024 complex; SW =64 kHz, 1376 scans	400 real; (TPPI) SW=81 kHz		60-degree sinebell; Lorentzian-to-Gaussian transformation	forward linear prediction of 1024 points; 60-degree sinebell; Lorentzian-to-Gaussian transformation
U-^{13}C,^{15}N-CA-SP1, NL4-3 A92E variant						
CP-DARR (τ_{mix}=50 ms)		1024 complex; SW = 64 kHz, 128 scans	512 real, SW = 45 kHz		30-degree sinebell; Lorentzian-to-Gaussian transformation	forward linear prediction of 512 points; 30-degree sinebell; Lorentzian-to-Gaussian transformation

direct-DARR(τ_{mix}=50 ms)		1024 complex; SW =64 kHz, 192 scans	400 real, SW = 45 kHz		30-degree sinebell; Lorentzian-to-Gaussian transformation	forward linear prediction of 512 points; 30-degree sinebell; Lorentzian-to-Gaussian transformation
NCACX		1024 complex; SW =85.2 kHz, 2048 scans	40 complex; (States) SW=6.5 kHz		30-degree sinebell; Lorentzian-to-Gaussian transformation	forward linear prediction of 64 points; 30-degree sinebell; Lorentzian-to-Gaussian transformation
NCA		1024 complex; SW =64 kHz, 320 scans	44 complex; (states) SW=6.5 kHz		30-degree sinebell; Lorentzian-to-Gaussian transformation	forward linear prediction of 128 points; 30-degree sinebell; Lorentzian-to-Gaussian transformation
NCOCX		1024 complex; SW =85 kHz, 2048 scans	40 complex; (TPPI) SW=65 kHz		30-degree sinebell; Lorentzian-to-Gaussian transformation	forward linear prediction of 128 points; 30-degree sinebell; Lorentzian-to-Gaussian transformation
CP-INADEQUATE		1024 complex; SW =64 kHz,512 scans	400 real; (TPPI) SW=81 kHz		60-degree sinebell; Lorentzian-to-Gaussian transformation	forward linear prediction of 1024 points; 60-degree sinebell; Lorentzian-to-Gaussian transformation
INADEQUATE		1024 complex; SW =64 kHz, 1376 scans	400 real; (TPPI) SW=81 kHz		60-degree sinebell; Lorentzian-to-Gaussian transformation	forward linear prediction of 1024 points; 60-degree sinebell; Lorentzian-to-Gaussian transformation
21.1 T						
U-^{13}C,^{15}N-CA, HXB2 variant						
CP-DARR (τ_{mix}=50 ms)		1536 complex; SW =100 kHz, 96 scans	400 real, SW = 45 kHz		30-degree sinebell; Lorentzian-to-Gaussian transformation	forward linear prediction of 400 points; 30-degree sinebell; Lorentzian-to-Gaussian transformation
NCA		1024 complex; SW =100 kHz, 360 scans	96 real; (TPPI) SW=7 kHz		30-degree sinebell; Lorentzian-to-Gaussian transformation	forward linear prediction of 256 points; 30-degree sinebell; Lorentzian-to-Gaussian transformation
NCACX		1024 complex; SW =100 kHz, 1200 scans	64 real; (TPPI) SW=5 kHz		30-degree sinebell; Lorentzian-to-Gaussian transformation	forward linear prediction of 64 points; 30-degree sinebell; Lorentzian-to-Gaussian transformation
NCACX (1)	1024 complex;	42 real; (TPPI)	40 real; SW=7	60-degree sinebell;	60-degree sinebell; Lorentzian-	forward linear prediction of 64

	SW =100 kHz, 1200 scans	SW=5 kHz	kHz	Lorentzian-to-Gaussian transformation	to-Gaussian transformation	points; 60-degree sinebell; Lorentzian-to-Gaussian transformation
NCACX (2)	1024 complex; SW =100 kHz, 144 scans	42 real; (TPPI) SW=5 kHz	40 real; SW=7 kHz	90-degree sinebell; Lorentzian-to-Gaussian transformation	forward linear prediction of 64 points; 90-degree sinebell; Lorentzian-to-Gaussian transformation	forward linear prediction of 64 points; 90-degree sinebell; Lorentzian-to-Gaussian transformation
NCOCX (1)	1024 complex; SW =100 kHz, 1200 scans	43 real; (TPPI) SW=5 kHz	24 real; SW=5 kHz	60-degree sinebell; Lorentzian-to-Gaussian transformation	forward linear prediction of 64 points; 60-degree sinebell; Lorentzian-to-Gaussian transformation	forward linear prediction of 64 points; 60-degree sinebell; Lorentzian-to-Gaussian transformation
NCOCX (2)	1024 complex; SW =100 kHz, 1200 scans	43 real; (TPPI) SW=5 kHz	24 real; SW=5 kHz	90-degree sinebell; Lorentzian-to-Gaussian transformation	forward linear prediction of 64 points; 90-degree sinebell; Lorentzian-to-Gaussian transformation	forward linear prediction of 64 points; 90-degree sinebell; Lorentzian-to-Gaussian transformation
CP-INADEQUATE		1536 complex; SW =100 kHz, 400 scans	207 real; (TPPI) SW=81 kHz		60-degree sinebell; Lorentzian-to-Gaussian transformation	forward linear prediction of 512 points; 60-degree sinebell; Lorentzian-to-Gaussian transformation
INADEQUATE		1536 complex; SW =100 kHz, 1200 scans	240 real; (TPPI) SW=81 kHz		60-degree sinebell; Lorentzian-to-Gaussian transformation	forward linear prediction of 512 points; 60-degree sinebell; Lorentzian-to-Gaussian transformation
21.1 T						
U-^{13}C,^{15}N-CA, HXB2 variant						
CP-DARR (τ_{mix}=50 ms)		1536 complex; SW =100 kHz, 96 scans	400 real, SW = 45 kHz		30-degree sinebell; Lorentzian-to-Gaussian transformation	forward linear prediction of 400 points; 30-degree sinebell; Lorentzian-to-Gaussian transformation
NCA		1024 complex; SW =100 kHz, 128 scans	80 real; (TPPI) SW=5kHz		30-degree sinebell; Lorentzian-to-Gaussian transformation	forward linear prediction of 256 points; 30-degree sinebell; Lorentzian-to-Gaussian transformation
direct-DARR(τ_{mix}=50 ms)		1536 complex; SW =100 kHz, 288 scans	176complex, SW = 45 kHz		30-degree sinebell; Lorentzian-to-Gaussian transformation	forward linear prediction of 256 points; 30-degree sinebell; Lorentzian-to-Gaussian transformation
CP-INADEQUATE		1536 complex; SW =100 kHz,	400 real; (TPPI) SW=81 kHz		60-degree sinebell; Lorentzian-to-Gaussian transformation	forward linear prediction of 1024 points; 60-degree sinebell;

	384 scans			Lorentzian-to-Gaussian transformation
INADEQUATE	1536 complex; SW =100 kHz, 1248 scans	240 real; (TPPI) SW=81 kHz	60-degree sinebell; Lorentzian-to-Gaussian transformation	forward linear prediction of 1024 points; 60-degree sinebell; Lorentzian-to-Gaussian transformation